ELSEVIER

Nuclear Instruments and Methods in Physics Research A 493 (2002) 121–130

NUCLEAR INSTRUMENTS & METHODS IN PHYSICS RESEARCH Section A

www.elsevier.com/locate/nima

Determination of energetic neutron spatial distribution using neutron induced nuclear recoil events

S.R. Hashemi-Nezhad[a,*], M. Dolleiser[a], R. Brandt[b], W. Westmeier[b,1], R. Odoj[c], M.I. Krivopustov[d], B.A. Kulakov[d,2], A.N. Sosnin[d]

[a] *Department of High Energy Physics, School of Physics, A28, University of Sydney, NSW 2006, Australia*
[b] *Institut für Physikalische, Kern- und Makromolekulare Chemie, FB 15, Philipps-Universität, Marburg, Germany*
[c] *Institut fuer Sicherheitsforschung und Reaktorsicherheit, Forschungszentrum Juelich GmbH, Juelich, Germany*
[d] *Joint Institute for Nuclear Research, JINR, Dubna, Russia*

Received 24 April 2002; received in revised form 16 July 2002; accepted 30 July 2002

Abstract

Neutron induced nuclear recoils were used to determine the spatial distribution of the weakly moderated spallation neutrons produced in the interaction of 1 GeV protons with lead and uranium–lead targets. CR39 plastic track detectors were used to record neutron-induced recoil tracks. The track density measurements were carried out using a fully automated optical microscope. The experimental results were compared with Monte Carlo simulations using MCNPX-2.1.5 code and an extension code that was written for this purpose. A good agreement was found between the experiment and calculations for normalised results. Applicability of the MCNPX-2.1.5 code for absolute recoil track density determination is discussed.

PACS: 25.40.Sc; 25.40.Dn; 87.66.−a; 29.85.+c

Keywords: Spallation neutrons; Neutron distribution; Recoil tracks; MCNPX code

1. Introduction

Neutron induced recoil events in different environments are used for the detection and spectroscopy of the energetic neutrons. In this work we use CR39 solid-state nuclear track detectors, SSNTD [1], to record and study the recoil events that were generated by spallation neutrons produced in the interaction of high energy protons with heavy metallic targets [2]. This type of SSNTD is widely used in fast neutron dosimetry studies [3–5].

One of the major shortcomings of the SSNTDs always has been the slowness of the track analysis and counting, especially when large sample sizes are involved. But nowadays this can be overcome by using a Fully Automated Optical Microscopes

*Corresponding author. Tel.: +61-2-9351-5964; fax: +61-2-9351-7727.

E-mail address: reza@physics.usyd.edu.au (S.R. Hashemi-Nezhad).

[1] Permanent address: Dr. Westmeier GmbH, 35085 Ebsdorfergrund, Germany.

[2] 1926–2002.

0168-9002/02/$ - see front matter
PII: S0168-9002(02)01551-6

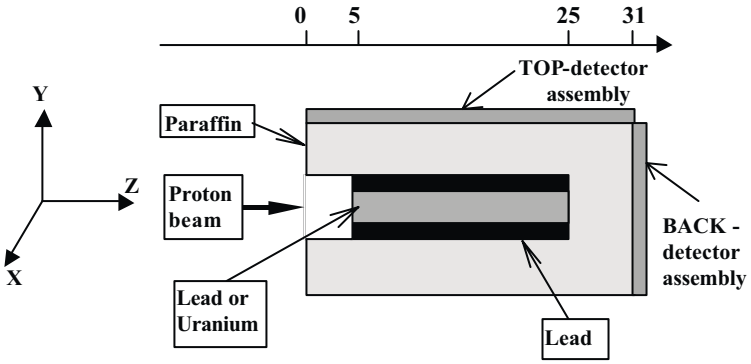

Fig. 1. Target-moderator and irradiation setup.

(FAOM). These instruments allow one to study the micro-distribution of the events of interest within macro-samples of SSNTDs.

Micro-spatial distribution studies of the fast neutron induced events are not readily feasible with electronics detectors unless one uses high-resolution detection systems such as solid-state pixel detectors (with appropriate converters). These are much more expensive and complicated hardware and software systems are required.

For quantitative assay it is important to simulate the response of the CR39 detectors with Monte Carlo (MC) methods, especially in connection with spallation neutrons and their applications in accelerator driven systems [6,7]. For this purpose we have employed one of the best and modern neutron transport codes namely MCNPX [8].

2. Experimental procedure

2.1. Irradiations

Two sets of detector assemblies were irradiated with weakly moderated spallation neutrons produced in the interaction of 1 GeV protons with Pb and U/Pb targets. The target moderator setups were similar to those used in earlier experiments (see e.g. [9–11]). Two types of targets were used, (a) a cylindrical lead target of diameter 8 and length 20 cm (Pb-target) and (b) two cylindrical uranium rods of diameter 3.6 cm and length 10.4 cm that were embedded in cylindrical lead shell of thickness 2.2 cm (U/Pb-target). The targets were surrounded with paraffin moderator of thickness 6 cm (Fig. 1).

We used plastic detectors to measure the spatial distributions of slow and energetic neutrons. For slow neutrons the detectors were cellulose nitrate foils coated with boron compound, LR-115 2B[3] and for the fast neutrons CR39 detectors were employed. Schematic drawing of the detector assemblies is shown in Fig. 2. The detector assemblies were placed on top of the paraffin moderator parallel to the axis of the target cylinder and in the back of the moderator normal to the target axis covering the centre of the back face. The detectors in top and back will be referred to as "Top" and "Back" detectors. The plastic detectors and Cd foils were 1.5 cm wide and 31 cm or 20 cm long for Top and Back detectors, respectively.

The detector assemblies were exposed to spallation (and fission) neutrons for the duration of one or two proton pulses in the target. The Synchrophasotron accelerator of Joint Institute for Nuclear Research (JINR), Dubna, Russia, provided the proton beam of energy 1 GeV. Total proton

[3] Manufactured by Kodak, Pathe, France.

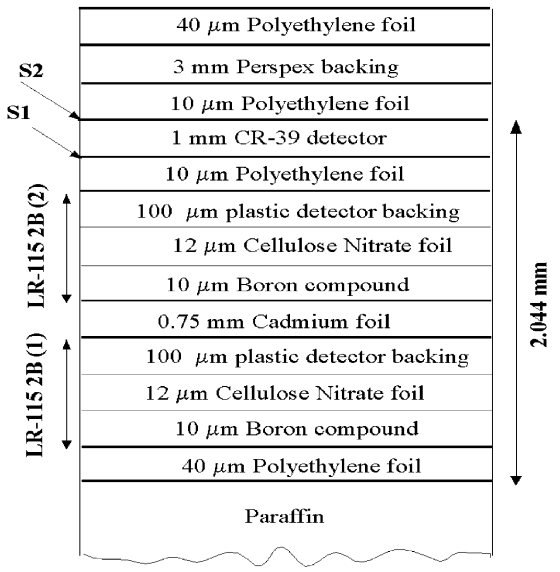

Fig. 2. Detector assembly.

fluence[4] for each irradiation was obtained from accelerator operators. The number of the protons that actually impinged on the targets was determined in the following manner.

After our short irradiation, other sensors were placed on the moderator (for another experiment) and proton irradiations were continued for much longer period to a total fluence of 10^{13}–10^{14} protons, using the same beam-target geometry as in the short irradiations. The number of protons on the target for these experiments was determined via radiochemical method as explained in Ref. [10]. We used the ratio of the radiochemically determined to the operator provided proton fluences to obtain an estimate of the proton fluence in the short irradiations. The resulting fluence values were $F_{U/Pb} = 6.2 \times 10^{10}$ and $F_{Pb} = 6.9 \times 10^{10}$ protons for U/Pb and Pb targets, respectively. The error in the radiochemical method of fluence determination is estimated to be $\sim 15\%$ [10].

2.2. Detector processing and track counting

In the present paper only the results of the Top CR39 detectors will be presented. The TASTRK^{TM} CR39[5] detectors were etched in 6 N NaOH at 70°C for a period of 6 h, along with separate CR39 samples that were irradiated with ^{252}Cf fission fragments. Measurements of the fission track diameters indicated a bulk etch rate of 1.3 μm h^{-1}.

The counting of the tracks was carried out using a Fully Automated Optical Microscope (FAOM) developed in the School of Physics, University of Sydney [12,13]. In the top detectors an area of the 0.5×31 cm^2 was scanned and results were stored in appropriate files. We counted the tracks in the back face of the CR39 detectors (marked S_2 in Fig. 2; the surface away from the paraffin moderator). The tracks observed on this surface of the detector result predominantly from the recoil events within the volume of the CR39 detector. In counting of the tracks a track contour area restriction of 2 μm^2 was imposed and the tracks with area less than this value were ignored.

Fig. 3 shows a photomicrograph of tracks (mainly; proton, carbon and oxygen recoil tracks) in the surface S_2 of the Top CR39 detector (Fig. 2), for the case of U/Pb target, at $Z \approx 11$ cm (cf. Fig. 1). The image dimension is 280×220 μm^2. The track density in this specific field of view is 860 tracks/mm^2 (corresponding to 53 tracks in the photomicrograph); there are no uncountable overlapping tracks in the field of view. For the samples studied in the present work, number of overlapped tracks was about 1%; majority of which could be distinguished and counted by FAOM with appropriate settings.

3. Monte carlo simulations

3.1. Recoils events

We used MCNPX 2.1.5 code [8] to obtain information on the recoil events within the volume of the CR39 detector ($C_{12}H_{18}O_7$; $\rho = 1.3$ g cm^{-3}). The target-moderator setup and detector assembly as shown in Figs. 1 and 2 were defined in the code,

[4] In this paper the term "fluence" is used to describe the time-integrated number of the protons that strike the target.

[5] CR39 detector, manufactured by H.H. Wills Physics Laboratory, University of Bristol, UK, under the trade name TASTRAK^{TM}.

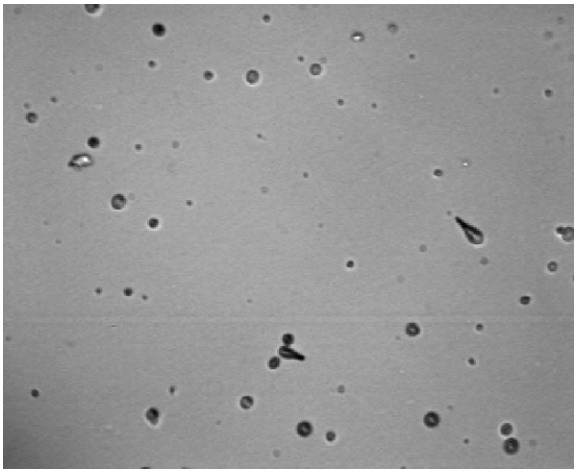

Fig. 3. Photomicrograph of recoil tracks (mainly proton, carbon and oxygen recoils) in TOP CR39 detector of the U/Pb irradiation at the location of $Z \cong 11$ cm (cf. Fig. 1). The image dimension is $280 \times 220\ \mu m^2$. The track density for this specific field of view is 860 tracks/mm^2 (corresponding to 53 tracks in the photomicrograph) and there are no uncountable overlapping tracks in this field of view. On average for these samples the number of the overlapping tracks is about 1% and majority of these can be distinguished and counted by FAOM with appropriate settings.

with the difference that in the calculations the detector assembly covered the whole surface of the moderator. This was done deliberately to increase the number of the recoil events per unit length of the detector cylinder and hence improve the statistics of the calculations. Such a setup to some extent will affect the slow neutron flux in the detector volume, however, it is not expected to influence the number or type of recoils in the CR39. In the simulations the target was "irradiated" with a proton beam of $E_p = 1$ GeV. The beam profile was elliptical with a Gaussian distribution in X- and Y-directions (Fig. 1) close to the beam shape in the actual experiment. In MCNPX calculations the high-energy data libraries [14] were used for the elements in the target–moderator–detector system except for uranium and cadmium for which such data library was not available. For these two elements the libraries provided by MCNP-4B2 [15] with an upper energy limit of 20 MeV were employed.

The particulars of the neutron collision events within the CR39 i.e. coordinates of the collision points, the participating nuclei, the direction cosines, energy and weight of the particles (i.e. the relative contribution of the particles to the final result [15]), were recorded in the PTRAC[6] file of the MCNPX 2.1.5.

In direct MC calculations without use of variance reduction techniques the statistics of the calculations was extremely poor and very high computing time was required. As a variance reduction method we used the forced collision [15] on the neutrons that enter the volume of the CR39 (cylindrical shell of inner radius 10.1044 cm, length 31 cm and thickness 0.1 cm). Also an energy cut-off of 0.1 MeV was imposed on the neutron activity within the CR39. These constrains improved the precision of the calculations dramatically for fewer incident proton histories and much shorter computer time. We used 5×10^5 incident proton histories, which resulted in a PTRAC file of size 711 MB in ASCII format.

Fig. 4 shows the variation of the number of recoil events (i.e. proton, carbon and oxygen recoils) in the detector volume as a function of distance from the beam axis. The number of recoil events within 1 mm thickness of the detector slightly decreases (at most $\sim 4\%$) with increasing distance from the beam-axis; which can be attributed to the normal neutron flux reduction with the distance.

We wrote an additional code, which uses the PTRAC as an input and transports the individual recoiling nuclei within the volume of the CR39 to the extent that either the recoiling nuclei stop within the detector or cross the desired surface. For range vs energy calculations the SRIM 2000.40 code was used [16]. The energy of the recoils, their coordinates at the exit point on the surface and angle of the recoils with respect to the detector surface (dip-angle) were calculated.

In order to decide which recoil will result in an etchable and detectable track the following restrictions were implemented in the code:

1. For the type of the detector and etching conditions used, in the case of the proton

[6] Default name for a file that can be produced by MCNP and MCNPX, which can contain information on e.g. collision events.

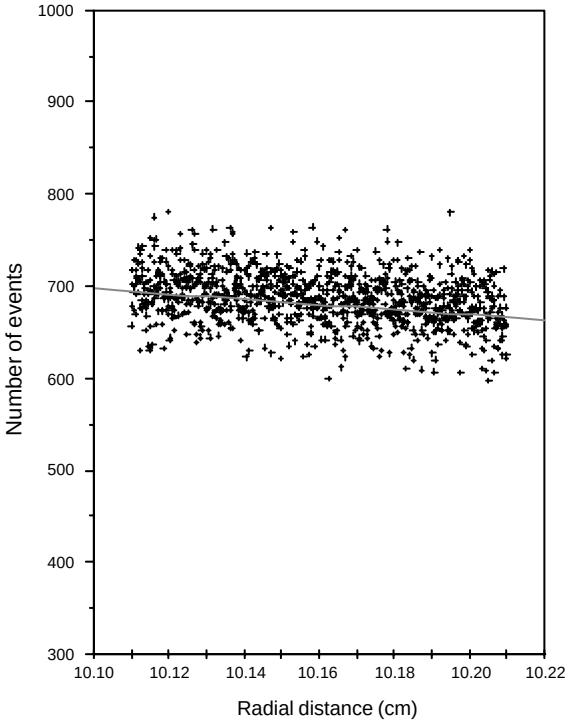

Fig. 4. Variation of the number of recoil events (i.e. proton, carbon and oxygen) in Top CR39 detector as a function of distance from the proton beam axis.

recoils only those, that their energy on exit from the surface S_2 were in the range of 100 keV to 2.5 MeV were considered [3], see also the condition 4 below.

2. For protons the critical dip angle θ_c [1], as function of proton energy E_r, was taken from Ref. [17] for proton recoil energies of $E_r \leqslant 700$ keV and from Ref. [18] for $E_r > 700$ keV.
3. In the case of the C and O recoils, no energy limits were imposed except the indirect lower energy limit that arises from the condition 4 below. Simulations showed that the total energy of the C and O recoils does not exceed 150 MeV. The critical angle for etched track formation $\theta_c(V)$, for these ions was calculated from following equations [19]:

$$\theta_C(V) = \sin^{-1}(1/V),$$

$$V \equiv V_t(\mathrm{LET}_\infty)/V_B = 1 + 1.136 \times \mathrm{LET}_\infty^{1.022}$$

where LET_∞ is the total linear energy transfer in units of MeV cm^2 mg^{-1} which was calculated using SRIM 2000.40 code [16], V_B is the bulk etch rate and V_t (LET_∞) is the track etch rate as a function of LET_∞.

4. For any type of recoil only those with a range $\geqslant 2$ μm in the detector were taken into account [3]. This condition sets the lower energy limits of 180 keV for protons, 1 MeV for C (83 keV/nucleon.) and 1.3 MeV for O-recoils (81 keV/nucleon).
5. A removed detector thickness (by etching) of $h = 7.8$ μm was taken into account.

Events satisfying all of the above conditions were binned along the beam axis using the coordinates at which recoils exist from the detector surface. The track density for each bin was calculated by taking into account the number of incident protons in the MC calculations, proton fluence during the experiment, and area of the each bin. It was found that in a detector of thickness 1 mm, on average 1.5% of proton recoils, 0.27% of carbon recoils and 0.2% of oxygen recoils within the detector volume resulted in etchable and detectable tracks.

Fig. 5 shows the calculated energy spectra of the neutrons and protons within the volume of the CR39. Neutron and proton spectra within the

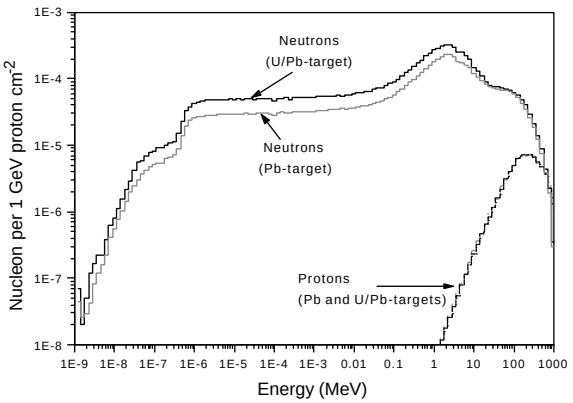

Fig. 5. Neutron and proton spectra within the volume of the Top CR39 detector. The proton distributions *do not* include those resulting from the recoil events. The protons in these spectra are produced in the course of the spallation process and nuclear reactions in the target–moderator–detector assembly.

volume of the Top CR39 detector. The proton distributions *do not* include those resulting from the recoil events. The protons in these spectra are produced in the course of the spallation process and nuclear reactions in the target-moderator-detector assembly (see Section 3.2). Note that the thermal peak in the neutron spectra is absent due to the presence of Cd in the detector assembly.

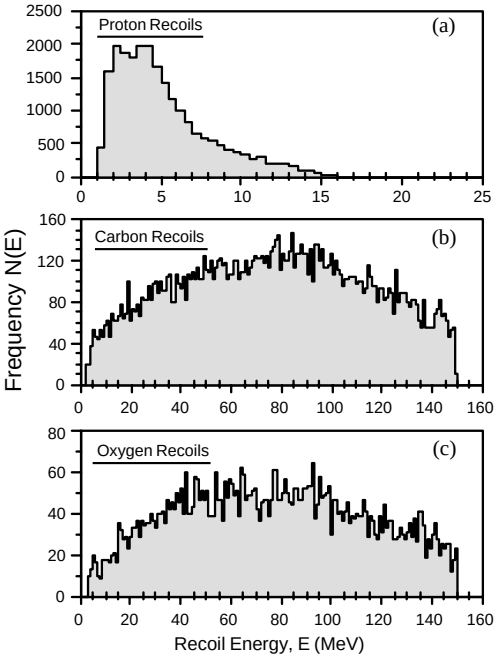

Fig. 6. Energy distribution of the proton, carbon and oxygen recoils within the volume of the TOP CR39 detector that resulted in etchable and detectable tracks in surface S_2. The distributions are for the Pb-target and the frequencies refer to 500 000 protons of energy 1 GeV on the target. The energy bin width for proton recoils is 0.5 and 1 MeV for C and O-recoils. Note that the energy on exit from the detector surface determines which recoil results in etechable and detectable track.

Fig. 6 illustrates the energy distributions of the proton, carbon and oxygen recoils in the detector volume. These are the recoil events that result in etchable and detectable tracks in the surface S_2 (see the figure caption for more details).

Table 1 shows the relative contributions of different nuclear species to the recoil events inside the detector volume and to the tracks on the surface. The similarities seen in Table 1 for U/Pb and Pb targets, is expected from the similarities of the neutron spectra within the CR39 for U/Pb and Pb targets (Fig. 5).

Calculations show that the simulated track densities are not very sensitive to the thickness of the layer removed from the detector during the etching process. This is expected, since majority of the neutrons in the location of the CR39 are moving in directions towards the outside of the setup (because of the small thickness of reflecting material beyond surface S_2) and for momentum conservation requirements, most of the recoils are also pointed towards the surface S_2. In other words prolonged etching does not enhance the track density significantly. This observation allows one to adjust the etching conditions to suit the track detection method employed.

Table 2 gives the MC-calculated recoil track production per neutron (for neutrons with energy spectra shown in Fig. 5). Track production per neutron in the case of the U/Pb target is slightly less than that for Pb-target. This is due to the fact

Table 1
MC results on the recoil event production in the 1 mm thick CR39 detector at $E_p = 1$ GeV

Type of recoil	U/Pb-target			Pb-target		
	Percentage of total recoils in the detector volume	Percentage of the total tracks	Mean range of recoils (μm)	Percentage of total recoils in the detector volume	Percentage of the total tracks	Mean range of recoils (μm)
Proton	33.04	80.41	129.3	27.68	77.17	150.7
Carbon	38.95	14.01	19.4	41.47	16.22	22.6
Oxygen	28.01	5.58	12.4	30.85	6.61	14.3

Table 2
Recoil track productions per neutron (of energy spectra given in Fig. 5) in the detector volume

Type of recoil-track	Recoil tracks per neutron (in the detector volume)	
	U/Pb-target	Pb-target
H	1.02×10^{-4}	1.16×10^{-4}
C	1.78×10^{-5}	2.41×10^{-5}
O	7.1×10^{-6}	9.81×10^{-6}
Total	1.27×10^{-4}	1.5×10^{-4}

that the relative number of the low energy neutrons (from spallation and fission processes) that do not contribute to the recoil track formation is larger for the case of the U/Pb target. The recoil track production rates that are given in Table 2 apply only to neutrons with energy spectra shown in Fig. 5 and may not be compared with track production efficiencies reported in literature for other neutron sources.

3.2. Tracks with non-recoil origin

Besides the neutron-initiated recoil events, the hydrogen and helium isotopes resulting directly from *spallation process* and those from the *nuclear reactions* can contribute to tracks recorded in the CR39.

With the available neutron and proton spectra (Fig. 5), energetically nuclear reactions, such as (x, p), (x, d), (x, t) (x, α) and (x, ^{3}He), (where x represents proton or neutron), with ^{12}C, ^{14}N and ^{16}O nuclei present in the detector assembly, are possible. The threshold energies for these reactions are in the range 2.4–21.4 MeV.

Fig. 7 shows the energy, spatial and angular distributions of the protons that *cross* the surface S_2 of the detector for the case of the U/Pb target, as calculated with the MCNPX 2.1.5 code. Distributions similar to those shown in Fig. 7 were also calculated for d, t, ^{3}He and ^{4}He ions.

It should be mentioned that the data libraries [14] treat recoil events as local energy dump and MCNPX 2.1.5 does not transport the recoiling nuclei. Thus the plots in Fig. 7 do not contain any

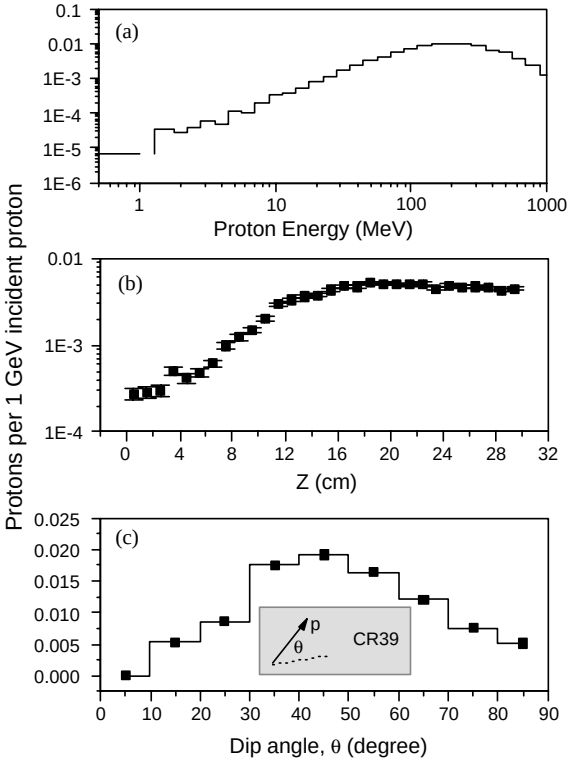

Fig. 7. Characteristics of the protons with non-recoil origin traversing the surface S_2 of the Top CR39 detector for the case of U/Pb-target: (a) energy distribution of the protons that cross surface S_2, (b) spatial distribution of the protons in surface S_2, and (c) distribution of the Dip angle of the protons that exit through surface S_2.

of the proton recoils within the target-moderator-detector setup. However, the p, d, t, ^{3}He and ^{4}He nuclei resulting from nuclear reactions are transported by MCNPX 2.1.5 and their contributions to the track densities can be estimated.

Using the information given in Fig. 7 (and those corresponding to ^{2}H and ^{3}H) and applying the same restrictions used for proton recoils, the contribution of the hydrogen isotopes to the track density at the surface S_2 in each bin was estimated and added to the recoil events. The calculations showed that at most 8% of the experimentally observed track densities at surface S_2 come from non-recoil H-isotopes. It was found that contributions of He-isotopes to the track density were negligible.

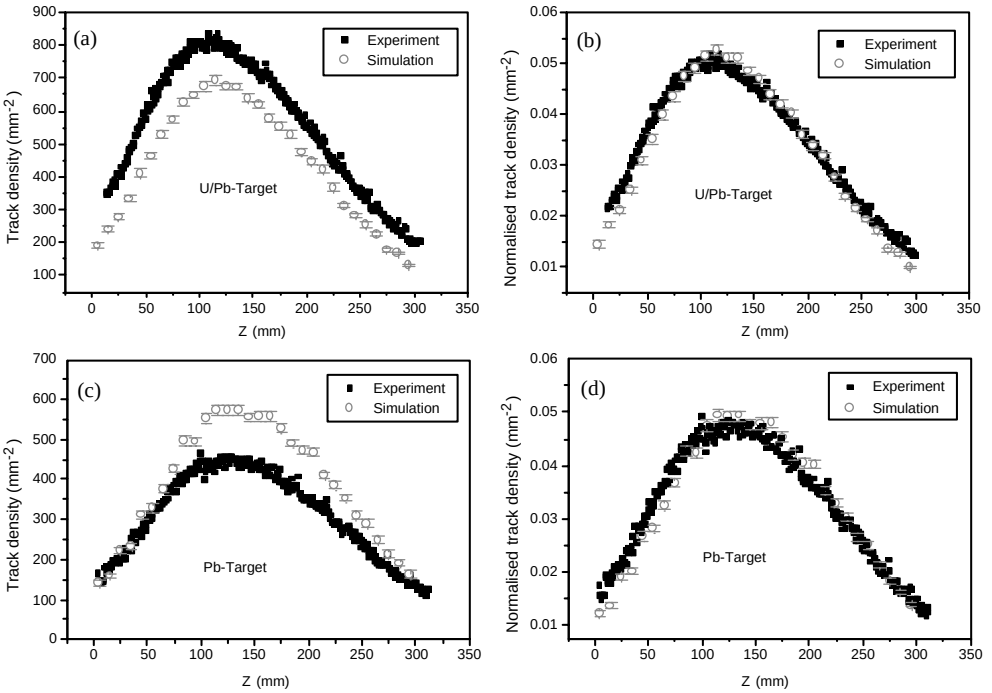

Fig. 8. Experimental and simulated spatial distribution of the tracks in TOP CR39 for U/Pb and Pb target–moderator systems. (a) and (c) Un-normalised results; (b) and (d) are normalised track density distributions.

4. Experimental results and discussion

Fig. 8 shows the experimental and simulated track density distributions for U/Pb and Pb-targets. Every experimental data point in Fig. 8 represents the average track density calculated from 125 fields of view, each covering an area of $\sim 0.2 \times 0.2\,\mathrm{mm}^2$ on the detector surface. All together in a given sample 38 500 fields of view were scanned. From Figs. 8a and c it can be seen that in the case of the U/Pb target, simulation underestimates (by $\sim 18\%$), while for Pb-target simulation overestimates (by $\sim 22\%$) track densities compared to the experimental observations.

The opposite trend of the disagreement between the experiment and simulation suggest that the differences do not come from the conditions imposed in the MC calculations but it must rather be due to parameters that are uniquely related to each experiment. Such parameters could be the proton fluence and/or counting efficiency of the FAOM. On the basis of repeated scanning of the samples and good reproducibility of the track densities it is clear that FAOM cannot be exclusively responsible for the observed discrepancies. Therefore, we believe that errors in the proton fluence determinations for our short irradiations (1–2 pulses) are the main source of the observed differences between experiments and simulations.

Figs. 8b and d show the normalised track density distributions for simulated and experimental results for U/Pb and Pb targets. As can be seen there is excellent agreement between the experiments and calculations for both target–moderator systems. Such an agreement between the normalised experimental and simulations results again suggest that the conditions used in the MC calculations cannot be the main reason for the observed discrepancies.

From Fig. 8 it can be seen that, the maximum of the track density distributions appears at different Z-values for the U/Pb and Pb targets. For U/Pb it is at $Z = 10.4$ cm corresponding to a depth of ~ 5 cm in the target while for Pb-target it appears

at $Z = 13$ i.e. 8 cm in the target. A similar effect has been reported in our earlier experiments [9] and also seen in these series of experiments for slow neutrons [20]. The position of the maximum is related to the maximum neutron yield per unit length of the target [2] and this position depends on proton energy E_p and on the target material.

If we assume that all of observed discrepancies between the experiment and calculations are due to the errors in the proton fluence determinations, then from the MC calculations and experimental results the proton fluences for U/Pb and Pb targets can be calculated as $F_{U/Pb} = 7.56 \times 10^{10}$ and $F_{Pb} = 5.57 \times 10^{10}$ protons, which are 18% higher and 23% lower than experimental fluence values respectively.

Although Figs. 8b and d suggest that the conditions used in the MC calculations are very close to reality they cannot be error-free. Thus the observed differences between the un-normalised experimental and simulation results are due to various approximations dominated by errors in the proton fluences.

5. Conclusions

Tracks in CR39 detector that mostly were produced by neutron induced recoils of the nuclei in the detector, were used to study the spatial distribution of spallation neutrons produced by 1 GeV protons in two types of target moderator systems. The MCNPX 2.1.5 code and a follow-up extension code were used to simulate the experimental results.

Within errors the MCNPX and the extension code correctly predict the position of the maximum and the overall shape of the track distributions and there is very good agreement between the normalised experimental and simulation results. However, the agreement for un-normalised results is not satisfactory. The observed discrepancies are associated mainly with errors in the values of the incident proton fluences, although errors in the conditions implemented in the MC calculations as well as errors associated with track counting can play a role.

To obtain statistically acceptable simulation results large number of proton histories must be followed and appropriate variance reduction techniques must be employed and as a result, very large size of PTRAC file (regardless of its format) is unavoidable. Even when the recoiling nuclei are transported with MCNPX, as will be the case in the future versions of this code [21], one still will require the PTRAC or a similar file to record the characteristics of the recoiling nuclei on exit from the desired surface.

References

[1] R.L. Fleischer, B.P. Price, R.M. Walker, Nuclear Tracks in Solids, University of California Press, Berkeley, CA, 1975.
[2] S.R. Hashemi-Nezhad, R. Brandt, W. Westmeier, V.P. Bamblevski, M.I. Krivopustov, B.A. Kulakov, A.N. Sosnin, J.-S. Wan, R. Odoj, Kerntechnik 66 (2001) 47.
[3] J. Palfalvi, L. Sajo-Bohus, Radiat. Meas. 28 (1997) 483.
[4] M. Luszik-Bhadra, E. Dietz, F. D'errico, S. Guldbakke, M. Matzke, Radiat. Meas. 28 (1997) 473.
[5] E. Vilela, E. Fantuzzi, G. Giacomelli, M. Giorgini, B. Morelli, L. Patrizii, P. Serra, V. Togo, Radiat. Meas. 31 (1999) 437.
[6] S.R. Hashemi-Nezhad, R. Brandt, W. Westmeier, V.P. Bamblevski, M.I. Krivopustov, B.A. Kulakov, A.N. Sosnin, J.-S. Wan, R. Odoj, et al. Monte Carlo calculations on transmutation of transuranic nuclear waste isotopes using spallation neutrons; difference of lead and graphite moderators. JINR Report E1-2000-291, 2000, and Nucl. Instr. and Meth. A 482 (2002) 547.
[7] S.R. Hashemi-Nezhad, R. Brandt, W. Westmeier, V.P. Bamblevski, M.I. Krivopustov, B.A. Kulakov, A.N. Sosnin, J.-S. Wan, R. Odoj, Monte Carlo studies of accelerator driven systems; energy and spatial distribution of neutrons in multiplying and mon-multiplying media. JINR Report E1-2000-291, 2001, and Nucl. Instr. and Meth. A 482 (2002) 537.
[8] Laurie S. Waters, Editor, MCNPX user's manual Ver. 2.1.5, TPO-E83-G-X-00001, Los Alamos National laboratory, November 1999.
[9] S.R. Hashemi-Nezhad, et al., Radiat. Meas. 31 (1999) 537.
[10] J.-S. Wan, M. Ochs, P. Vater, X.P. Song, E.-J. Langrock, R. Brandt, J. Adam, V.P. Bamblevski, B.A. Kulakov, M.I. Krivopustov, A.N. Sosnin, G. Modolo, R. Odoj, Nucl. Instr. and Meth. B 155 (1999) 110.
[11] J.-S. Wan, et al., Nucl. Instr. and Meth. A 463 (2001) 634.
[12] S.R. Hashemi-Nezhad, M. Dolleiser, Radiat. Meas. 28 (1997) 836.

[13] M. Dolleiser, S.R. Hashemi-Nezhad (2002), A fully automated optical microscope for particle track analysis in solids, Nucl. Instr. and Meth. B, 2002, in press.
[14] M.B. Chadwick, P.G. Young, S. Chiba, S.C. Frankle, G.M. Hale, H.G. Hughes, A.J. Koning, R.C. Little, R.E. MacFarlane, R.E. Prael, L.S. Waters, Nucl. Sci. Eng. 131 (3) (1999) 293.
[15] J.F. Briesmeister (Ed.), MCNP-4B2—A general Monte Carlo N-particle transport code, Report LA-12625-M, Los Alamos National laboratory, March 1997.
[16] J.F. Ziegler, J.P. Biersack, U. Littmark, The stopping and range of ions in matter, Pergamon Press, Oxford, 1985. (calculations were performed with SRIM-2000 version 40, see www.SRIM.org.)
[17] A. Waheed, G. Moschini, H.A. Khan, R. Cherubini, L. Lembo, A.M.I. Haque, Nucl. Tracks Radiat. Meas. 15 (1988) 129.
[18] Matiullahand, S.A. Durrani, Nucl. Tracks Radiat. Meas. 15 (1988) 203.
[19] A.N. Golovchenko, et al., Radiat. Meas. 28 (1997) 455.
[20] S.R. Hashemi-Nezhad, 2001, unpublished.
[21] L.S. Waters, Los Alamos National Laboratory, private communications.